

SOLAR: Second-Order Loss and Attention for Image Retrieval

Tony Ng^{1,2} Vassileios Balntas² Yurun Tian¹ Krystian Mikolajczyk¹

¹Imperial College London

²Scape Technologies

{tony.ng14, y.tian, k.mikolajczyk}@imperial.ac.uk

vassileios@scape.io

Abstract

Recent works in deep-learning have shown that utilising second-order information is beneficial in many computer-vision related tasks. Second-order information can be enforced both in the spatial context and the abstract feature dimensions. In this work we explore two second order components. One is focused on second-order spatial information to increase the performance of image descriptors, both local and global. More specifically, it is used to re-weight feature maps, and thus emphasise salient image locations that are subsequently used for description. The second component is concerned with a second-order similarity (SOS) loss, that we extend to global descriptors for image retrieval, and is used to enhance the triplet loss with hard negative mining. We validate our approach on two different tasks and three datasets for image retrieval and patch matching. The results show that our second order components bring significant performance improvements in both tasks and lead to state of the art results across the benchmarks.

1. Introduction

Self-attention mechanisms in form of non local blocks showed success originally in natural-language processing [49]. Their introduction to computer-vision related tasks in [50], led to improvements in video classification and object detection. Following works have also advanced other areas by using non-local blocks in fields such as GANs [54], semantics segmentation [55], and person-reID [51]. While recent methods in deep-learning based global descriptors for image retrieval have introduced more efficient ways to aggregate features into a global representation, they have not explored the correlations between features within a feature map. In this work we aim to exploit the second-order relationships between features at different spatial locations and combine with second-order descriptor similarity to the problem of feature descriptors for image retrieval and matching.

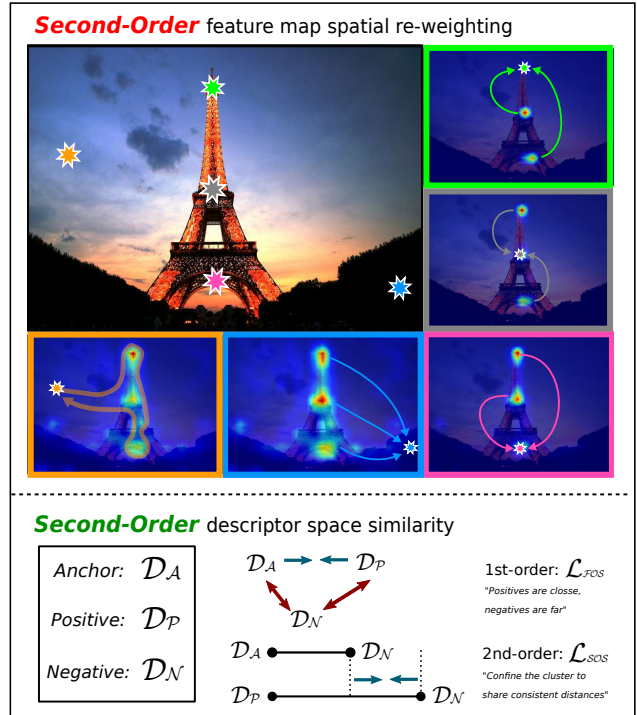


Figure 1. Illustration of our proposed SOLAR (Second-Order Loss and Attention for image Retrieval) descriptor. **Top.** We exploit second-order information through spatial self-attention, re-weighting the feature maps to give a better global representation of the image. **Bottom.** We also apply second-order similarity of learning descriptor distances during training of SOLAR.

Our main contributions are the following:

- We combine second-order spatial attention and second-order feature descriptor loss to improve image description for retrieval and matching.
- We show how to combine second-order attention for consecutive feature maps at different resolution to obtain the best descriptions and we perform a thorough ablation study on its effects.
- We show that the combination of second-order spatial in-

formation and descriptor similarity generalises well on both local and global descriptor learning.

d) We validate our proposed method with extensive evaluation on three benchmarks for image retrieval and matching, showing significant improvements compared to the state of the art.

2. Related work

Methods for image retrieval [2, 16, 32, 33, 34] and place recognition [3, 10, 28] can be loosely divided into two categories: *local aggregation* and *global single-pass*. Most methods prior to the deep-learning dominance [11, 14, 21, 39] were based on *local aggregation*, e.g. Bag-of-Words (BoW) [40] which aggregates a set of handcrafted, SIFT-like [8, 22] local features into a global representation [15, 16, 17, 18, 32, 33, 40, 45, 47]. While many of the *local aggregation* methods carried-over into the deep-learning era [28, 41, 42], the rise of CNNs [14, 21, 39] with highly expressive feature maps [11] provided an effective approach for global descriptor generation. Early attempts were mostly hybrid methods by exploring CNN features as analogous to local descriptors and aggregating them with similar techniques [1, 4, 41]. Later works showed that feature vectors from CNN feature maps can be combined into a global descriptor in a *single-pass* through various pooling operations [13, 35, 36, 48] while matching the level of performance from *local aggregation* methods. These methods fall into the *global single-pass* category.

Local aggregation methods generally consist of two steps. First, local features are detected and described. These can come in the form of early hand-crafted features such as SIFT [22] and SURF [8], or later in the form of CNN-based local descriptors [4, 28]. Second, the collection of local descriptors is compiled into a compact vector representation. Early works on BoW assigned local descriptors to visual words through various size codebooks [40]. These visual words are then encoded with matching techniques e.g. Hamming Embeddings [16], Fisher Kernels [30, 31] and Selective Match Kernels [45]; or with aggregation techniques e.g. k-means [27, 32] and VLAD [17, 18] to produce a compact descriptor vector. With the new-found success of CNN-based local descriptors [43, 44, 53], the classical SIFT-based features were replaced with learnt features [4, 26, 28, 12] which lead to substantial improvements in image retrieval, especially for large-scale and challenging datasets [28, 34]. These hybrid methods also used learnt local to global encoding schema [1, 5]. Recent system for large-scale image retrieval [42] aggregates local features from regions-of-interest (RoIs) detected by a separate network [37]. It was shown that the performance gain is largely due to filtering out irrelevant features such as background and moving objects.

Global single-pass methods, as opposed to *local aggregations*, do not separate the local feature extraction and aggregation steps. Instead, a global descriptor is generated by a single forward-pass through a CNN. Notice that even though hybrid methods use CNN features as local descriptors followed by *local aggregations* [1, 26], thus generate the global descriptor through a forward-pass of a CNN, we do not consider such methods as strictly *global single-pass*. This is because the final global descriptor is obtained through a handcrafted encoding schema rather than learnt in end-to-end manner. In order to aggregate the feature map output from a CNN, either Off-the-Shelf [11] or fine-tuned on retrieval-specific datasets [36], a global pooling operation must be included. The varieties of different *global single-pass* methods differ mostly on this pooling operation, which comes in the form of max-pooling [48], SPoC [4], CroW [19], R-MAC [48] and GeM [36]. GeM [36] is the most superior method amongst all due to its flexibility in weighting feature vectors according to their activations. Revaud *et al.* [38] recently achieved state-of-the-art results on image retrieval across *global single-pass* for introducing a loss directly learning on the average-precision metric, with GeM as the pooling method.

While second-order spatial attention mechanisms has shown success in natural-language processing [49] and various computer-vision tasks such as video understanding [50], GANs [54], semantics segmentation [55], person-reID [51], it is still a very young technique and has yet been applied to visual representation and descriptor learning. On the other hand, second-order loss has only recently been introduced to representation learning [44] on local patches by confining the second-order distance in clusters to be similar. To our best knowledge, our work is the first to demonstrate second-order spatial attention in descriptor learning and combine with second-order descriptor loss in learning global descriptors for image retrieval.

3. Method

3.1. Preliminaries

For an input image $I \in \mathbb{R}^{H,W,3}$ with feed-forward through a Fully-Convolutional Network (FCN) denoted by θ , we obtain the final feature map $\mathbf{f} = \theta(I) \in \mathbb{R}^{h,w,d}$ where h, w are the height and width of the feature map and d is the feature dimensionality. For $h, w > 1$, Radenović *et al.* [36] introduced the Generalised-Mean (GeM) pooling as a flexible way to aggregate the feature map into a single feature vector \mathbf{D}_g . The GeM pooling operation is defined as

$$\text{GeM}(\mathbf{f}, p) = \left(\frac{1}{N} \sum_{i=0}^N f_i^p \right)^{\frac{1}{p}}, \quad (1)$$

where p is a learnable parameter.

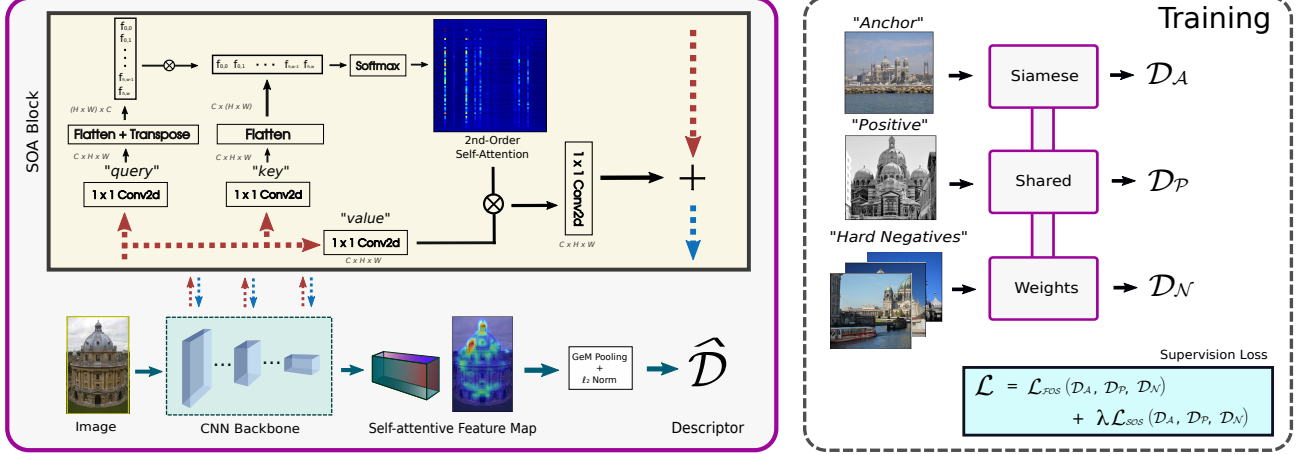


Figure 2. Overall pipeline for the proposed global descriptor. We perform Second Order Loss and Attention for image Retrieval (SOLAR) by inserting a number of Second Order Attention (SOA) blocks into different feature map levels of a CNN backbone, followed by GeM [36] pooling and ℓ_2 normalisation. We train SOLAR utilising a triplet network with an objective loss combining first-order and second-order descriptor losses.

3.2. Second-order spatial pooling

While the p -norm is able to control the share of contribution of each feature vector $f_k \in \mathbf{f}$ into the global descriptor \mathbf{D}_g , for FCNs it has a limited receptive field projected back to the original image. Let the center of each pixel location (i, j) in \mathbf{f} projected onto the original image to be at (i_0, j_0) . Assuming a rectangular receptive field $R = [R_x, R_y]$, each neuron $f_{ij} \in \mathbf{f}$ is strictly a function of the receptive field, as a set of pixels

$$f_{ij} = \theta \left(\left\{ I_{\mathcal{P}} \in I \mid |\mathcal{P}_i - i_0| \leq R_x \wedge |\mathcal{P}_j - j_0| \leq R_y \right\} \right), \quad (2)$$

where \mathcal{P} is the set of pixel locations in I .

To incorporate second-order spatial information into the feature pooling, we use the non-local block [50] shown in Figure 2. By applying `flatten` to the *query* and *key* heads of \mathbf{f} , each obtained through 1×1 convolutions, we have two tensors \mathbf{q}, \mathbf{k} of shape $N \times d$, where $N = h \times w$. A second-order self-attention map is then computed through

$$\mathbf{z} = \text{softmax}(\alpha \cdot \mathbf{q}^T \mathbf{k}), \quad (3)$$

where α is a scaling factor. This results in a self-attention map with dimensionality $N \times N$, meaning that for each f_{ij} it contains the information from the whole feature map \mathbf{f} . Lastly, \mathbf{f} is *re-weighted* through the matrix multiplication

$$\mathbf{f}^{so} = \mathbf{f} + \psi(\mathbf{z} \otimes \mathbf{v}) \quad (4)$$

where \mathbf{v} is the *value* head also through 1×1 convolution and ψ is another 1×1 convolution to control the scale of the feature map re-weighting. Now, each feature vector f_{ij}^{so} in the newly second-order re-weighted \mathbf{f}^{so} is a function and

contains information from all other pixel locations of \mathbf{f}

$$f_{ij}^{so} = g(\mathbf{z}_{ij} \odot \mathbf{f}), \quad (5)$$

where g denotes the collection of all convolutional operations within the non-local block. Now if we denote the new FCN with the added non-local block(s) with ϕ , each neuron is a function of the full image $f_{ij}^{so} = \phi(\{I_{\mathcal{P}} | I\})$ and the corresponding GeM-pooling

$$\text{GeM}(\mathbf{f}^{so}, p) = \left(\frac{1}{N} \sum_{i=0}^N f_i^{so^p} \right)^{\frac{1}{p}} \quad (6)$$

is spatially second-order rich in information. We refer to this block as the **Second-Order Attention (SOA)** block throughout the rest of the paper.

3.3. Second-order similarity distance loss

First-order similarity. With the abundance of large-scale labelled training datasets [42], the triplet loss is a standard for learning first-order descriptor distances [7, 24, 43]. Given an anchor, positive and negative forming the triplet, their respective global descriptors are $\mathbf{D}_a, \mathbf{D}_p, \mathbf{D}_n$, the triplet loss which is first-order in descriptor space is

$$\mathcal{L}_{FOS} = \max(\|\mathbf{D}_a - \mathbf{D}_p\|^2, \|\mathbf{D}_a - \mathbf{D}_n\|^2 + m), \quad (7)$$

where m is the margin.

Second-order similarity. Following SOSNet [44], the second-order similarity regularisation loss can be applied to global descriptors in a similar fashion. We hard-mine negative pairs as in [36] and the SOS loss is

$$\mathcal{L}_{SOS} = (\|\mathbf{D}_a - \mathbf{D}_n\|^2 - \|\mathbf{D}_p - \mathbf{D}_n\|^2)^{\frac{1}{2}}. \quad (8)$$

	Method	Medium								Hard							
		\mathcal{ROxf}		$\mathcal{ROxf}+\mathcal{R1M}$		\mathcal{RPar}		$\mathcal{RPar}+\mathcal{R1M}$		\mathcal{ROxf}		$\mathcal{ROxf}+\mathcal{R1M}$		\mathcal{RPar}		$\mathcal{RPar}+\mathcal{R1M}$	
		mAP	mP@10	mAP	mP@10	mAP	mP@10	mAP	mP@10	mAP	mP@10	mAP	mP@10	mAP	mP@10	mAP	mP@10
Local Agg.	HesAff-rSIFT-ASMK* [46]	60.4	85.6	45.0	76.0	61.2	97.9	42.0	95.3	36.4	56.7	25.7	42.1	34.5	80.6	16.5	63.4
	DELf-ASMK* (reimpl.) [42]	65.7	87.9	–	–	77.1	98.7	–	–	41.0	57.9	–	–	54.6	90.9	–	–
	DELf-D2R-R-ASMK* [42]	69.9	89.0	–	–	78.7	99.0	–	–	45.6	61.9	–	–	57.7	93.0	–	–
	— DELf [GL18] [42]	73.3	90.0	61.0	84.6	80.7	99.1	60.2	97.9	47.6	64.3	33.6	53.7	61.3	93.4	29.9	82.4
Global Single-Pass	AlexNet-GeM [36]	43.3	62.1	24.2	42.8	58.0	91.6	29.9	84.6	17.1	26.2	9.4	11.9	29.7	67.6	8.4	39.6
	VGG16-GeM [36]	61.9	82.7	42.6	68.1	69.3	97.9	45.4	94.1	33.7	51.0	19.0	29.4	44.3	83.7	19.1	64.9
	ResNet101-R-MAC [13]	60.9	78.1	39.3	62.1	78.9	96.9	54.8	93.9	32.4	50.0	12.5	24.9	59.4	86.1	28.0	70.0
	ResNet101-SPoC [4] [O]	39.8	61.0	21.5	40.4	69.2	96.7	41.6	92.0	12.4	23.8	2.8	5.6	44.7	78.0	15.3	54.4
	ResNet101-CroW [19]	41.4	58.8	22.5	40.5	62.9	94.4	34.1	87.1	13.9	25.7	3.0	6.6	36.9	77.9	10.3	45.1
	ResNet101-GeM [36] [O]	45.8	66.2	25.6	45.1	69.7	97.6	46.2	94.0	18.1	31.3	4.7	13.4	47.0	84.9	20.3	70.4
	ResNet101-GeM [52]	64.7	84.7	45.2	71.7	77.2	98.1	52.3	95.3	38.5	53.0	19.9	34.9	56.3	89.1	24.7	73.3
	ResNet101-GeM+DAME [36]	65.3	85.0	44.7	70.1	77.1	98.4	50.3	94.6	40.4	56.3	22.8	35.6	56.0	88.0	22.0	69.0
	ResNet101-GeM+AP [38]	67.5	–	47.5	–	80.1	–	52.5	–	42.8	–	23.2	–	60.5	–	25.1	–
	ResNet101-GeM [36] [GL18]	67.3	84.7	–	–	80.6	96.7	–	–	44.3	59.7	–	–	61.5	90.7	–	–
	Ours																
	ResNet101-GeM+SOA†	68.6	85.7	–	–	81.4	96.6	–	–	46.9	62.7	–	–	63.7	91.9	–	–
	ResNet101-GeM+SOLAR†	69.9	86.7	53.5	76.7	81.6	97.1	59.2	94.9	47.9	63.0	29.9	48.9	64.5	93.0	33.4	81.6

Table 1. Large-scale image retrieval results of our proposed second-order method against state-of-the-arts on the \mathcal{ROxf} - \mathcal{RPar} [34] and the respective 1 million distractors dataset. We evaluate against the *Medium* and *Hard* protocols on the mAP and mP@10 metrics. For *global single-pass* methods, the first word is the backbone CNN architecture used. [O] denotes results from ImageNet off-the-shelf networks. ResNet101-GeM [GL18] is the results from newly trained model released by [36]’s authors. Our method uses the ResNet101 with SOA† denoting the best configuration described in Table 2. SOLAR† is the full proposed method including the Second-Order similarity Loss.

Combining with second-order spatial reweighting, the final objective function is

$$\mathcal{L} = \mathcal{L}_{FOS} + \lambda \mathcal{L}_{SOS}, \quad (9)$$

where λ is a hyperparameter for weighting between the two loss terms.

3.4. Descriptor whitening

Descriptor whitening is crucial to improving the quality of descriptors. While the original work in GeM [36] used a linear projection for descriptor whitening [23], updated experiments¹ show superior results with whitening learnt end-to-end. We follow this new approach, inserting a bias-enabled fully-connected layer after GeM pooling and ℓ_2 -norm and train it end-to-end.

3.5. Network architecture and training

The pipeline of our proposed method is shown in Figure 2. The SOA blocks are insert-able at any (including intermediate) feature maps as it serves the function of feature reweighting. During training we adopt the Siamese network approach, *i.e.* all the triplets are passed into shared weight networks. Hard-negatives mining is also performed at the start of every epoch from a random pool of negatives and it is made sure that no negatives from each scene are from the same cluster, so to ensure higher sample variability from within the mini-batch. Details are described in Section 6.

¹github.com/filipradenovic/cnnimageretrieval-pytorch

4. Results on large-scale image retrieval

4.1. Datasets

In this section, we present results of SOLAR on large-scale image retrieval task and compare it with existing state-of-the-art results that do not exploit second-order information at training.

Google Landmarks 18 (GL18) [42] is an extension to the original Google Kaggle landmark recognition and retrieval challenge [28] dataset. It contains over 1.2 million internet photos from 15k landmarks around the world. These landmarks cover a wide-range of classes from historic cities to modern metropolitan areas to nature sceneries. GL18 also contains over 80k bounding boxes singling out the most prominent landmark in each image. In this work it serves as a semi-automatically labelled data-rich training set for image retrieval.

Revisited Oxford and Paris [34] is the commonly used dataset for evaluating the performance of global descriptors on large-scale image retrieval tasks. Radenovic *et al.* recently revisited the Oxford [32] and Paris [33] buildings by removing past annotation errors and adding new images. The Revisited-Oxford (\mathcal{ROxf}) and Revisited-Paris (\mathcal{RPar}) datasets contain 4,993 and 6,322 database images respectively, and each with 70 query images with a bounding box depicting the most prominent landmark in that query. Evaluation protocol are divided into three difficulties – *Easy*, *Medium* and *Hard* and the mean average precision (mAP) and mean precision at rank 10 (mP@10) are usually re-

ported as evaluation metrics. There is a supplementary 1M-distractor ($\mathcal{R}1\text{M}$) database set that contains one million extra distractor images to further test the robustness of the global descriptors. The $\mathcal{R}1\text{M}$ set is also evaluated with the same protocols and metrics as in $\mathcal{R}\text{Oxf}$ - $\mathcal{R}\text{Par}$.

4.2. Comparison against state-of-the-art

We compare SOLAR against other state-of-the-art image retrieval methods on the $\mathcal{R}\text{Oxf}$ - $\mathcal{R}\text{Par}$ [34] evaluation datasets and results are presented in Table 1. By adding SOA blocks, we achieve state-of-the-art mAP and mP@10 performance, by a large margin, when compared to all other *global single-pass* methods, on both datasets for both *Medium* and *Hard* protocols (with the exception of mP@10 in $\mathcal{R}\text{Par}$ -*Medium*). With the additional exploitation of Second-Order Loss (denoted by SOLAR †), the results are further improved by 1%. When compared with the baseline (Resnet101-GeM [GL18] [36]), SOLAR outperforms in mAP on the most challenging *Hard* protocol for $\mathcal{R}\text{Oxf}$ and $\mathcal{R}\text{Par}$ with a significant 3.6% and 3.0% gain respectively, as well as 3.3% and 2.7% on mP@10. Our method also outperforms the current state-of-the-art *local aggregation* method of DELF-D2R-R-ASMK* in mAP on $\mathcal{R}\text{Oxf}$ -*Hard*, $\mathcal{R}\text{Par}$ -*Medium* and *Hard* by 0.3%, 0.9% and 3.2%. It should be noted that the memory consumption for *local aggregation* descriptors is much higher than for *global single-pass* (27.6GB as reported in DELF-D2R-R-ASMK* [42] vs. 8.2GB for GeM [36] descriptors in the $\mathcal{R}1\text{M}$ distractors set). SOLAR also runs in a significant faster speed compared to DELF-D2R-R-ASMK* (0.15s processing time per image vs. >1.5s on a Titan Xp GPU). The SOA blocks in SOLAR only cause a negligible 7.4% overhead in terms of inference time.

The specific choice of SOA blocks insertion is justified in Section 5.1 through a detailed ablation study.

5. Ablation study

In this section we present thorough results of the impact of SOA on descriptor generation. We first show how different SOA insertions affect the image retrieval results. Then we explore how to exploit second-order spatial information to generate better descriptors using local patches as an example. This shows that SOLAR generalises to both local and global descriptors.

5.1. Impact of SOA on image retrieval

The results in Section 4.1 show that by simultaneously exploiting second-order spatial information through the SOA blocks and second-order descriptors distance information through the SOS loss, we greatly improve the performance of descriptor generation for image retrieval. To understand more deeply how each of SOA re-weighting affects the quality of global descriptors, we present an abla-

	Medium		Hard	
	$\mathcal{R}\text{Oxf}$	$\mathcal{R}\text{Par}$	$\mathcal{R}\text{Oxf}$	$\mathcal{R}\text{Par}$
ResNet101-GeM (baseline)	67.3	80.6	44.3	61.5
ResNet101-GeM+SOA ₄	68.2	81.0	45.7	62.3
ResNet101-GeM+SOA ₅	68.3	81.3	45.9	62.8
ResNet101-GeM+SOA _{4,5}	68.6	81.6	46.9	63.7

Table 2. Ablation study of SOA blocks on large-scale image retrieval [34]. We use backbone of ResNet101+GeM-pooling [36] and add SOA blocks after `conv_4x` and `conv_5x` in ResNet. Results are reported in mAP for the *Medium* and *Hard* protocols.

tion study on the CNN backbone in Section 4.1 to investigate particularly the impact of second-order spatial information. In Table 2 we show the impact of SOA insertion at different layers of a deep CNN. We follow [36] in using ResNet101 [14] fine-tuned on the GL18 dataset [42] as the baseline. ResNet101 contains 5 fully-convolutional blocks `conv1` to `conv5_x`. For retrieval the input image usually has high resolution (1000+ pixels on longer side), inserting SOA blocks before `conv4_x` is computationally too expensive to train at a reasonable time and memory consumption given the $O(n^2)$ complexity of Equation 3. From Table 2, our proposed SOA insertion improves retrieval mAP for 0.93%, 1.15% and 1.78% for SOA₄, SOA₅, and SOA_{4,5} respectively. This shows that the addition of consecutive SOAs is beneficial. We observe that the improvement brought by fine-tuning on SOA₅ is higher than SOA₄. One potential explanation is as follows: assume an input image of 1024×1024 pixels, the feature maps of ResNet after `conv4_x` and `conv5_x` have spatial resolutions of 64×64 and 32×32 respectively. Therefore even at the last feature map the spatial second-order information is still rich and fine-grained compared to say, for local patches (to be explained in the next Section 5.2). As SOA₅ re-weights the last feature map for GeM pooling, it injects second-order spatial information more directly into the global descriptor, resulting in better relative performance.

5.2. Generalisation to local patch descriptor

To validate the generalisation ability of our proposed method besides global descriptors, we further test it on local descriptors learning. Local patches have different statistics than global images, containing less semantic but more repeatable structures *e.g.* corners or blobs. However, local descriptors matching shares the same essence with image retrieval. Therefore, we train a local descriptor network with the proposed second-order spatial attention.

SOSNet [44] provided a holistic view on how second-order information in the descriptor space could be exploited for better patch descriptor. Hence, it is straightforward to directly insert SOA blocks into SOSNet to demonstrate that the idea of exploiting both second-order spatial information

Train		Liberty		Notredame		Yosemite		
Test	Extra Params	Notredame	Yosemite	Liberty	Yosemite	Liberty	Notredame	Mean
SOSNet	–	1.95	0.58	1.25	1.25	2.84	0.87	1.46
SOSNet+ (<i>reimpl.</i>)	–	1.31 \pm 0.01	0.46 \pm 0.04	1.21 \pm 0.06	1.07 \pm 0.03	2.25 \pm 0.03	0.80 \pm 0.04	1.138 \pm 0.034
SOSNet+, SOA ₃	12,288	1.22 \pm 0.04	0.45 \pm 0.03	1.20 \pm 0.03	0.96 \pm 0.05	2.01 \pm 0.10	0.73 \pm 0.04	1.065 \pm 0.050
SOSNet+, SOA ₄	12,288	1.27 \pm 0.04	0.44 \pm 0.03	1.23 \pm 0.06	0.99 \pm 0.09	2.08 \pm 0.01	0.78 \pm 0.01	1.130 \pm 0.040
SOSNet+, SOA ₅	22,528	1.26 \pm 0.03	0.44 \pm 0.02	1.17 \pm 0.02	0.99 \pm 0.06	2.06 \pm 0.04	0.73 \pm 0.02	1.108 \pm 0.031
SOSNet+, SOA ₆	22,528	1.30 \pm 0.02	0.56 \pm 0.05	1.23 \pm 0.07	1.59 \pm 0.08	2.80 \pm 0.05	0.93 \pm 0.01	1.380 \pm 0.046
SOSNet+, SOA _{3,4}	24,576	1.21 \pm 0.02	0.42 \pm 0.03	1.15 \pm 0.02	1.00 \pm 0.01	2.07 \pm 0.01	0.75 \pm 0.06	1.101 \pm 0.040
SOSNet+, SOA _{3,5}	24,576	1.27 \pm 0.06	0.45 \pm 0.05	1.30 \pm 0.02	0.96 \pm 0.03	2.19 \pm 0.02	0.82 \pm 0.01	1.139 \pm 0.030
SOSNet+, SOA _{4,5}	34,816	1.22 \pm 0.03	0.48 \pm 0.01	1.29 \pm 0.01	0.97 \pm 0.01	2.22 \pm 0.04	0.75 \pm 0.04	1.130 \pm 0.021
SOSNet+, SOA _{4,6}	34,816	1.39 \pm 0.02	0.59 \pm 0.02	1.59 \pm 0.19	1.32 \pm 0.03	2.72 \pm 0.18	0.89 \pm 0.03	1.416 \pm 0.077
SOSNet+, SOA _{3,4,5}	47,104	1.32 \pm 0.03	0.46 \pm 0.02	1.36 \pm 0.04	1.02 \pm 0.10	2.10 \pm 0.06	0.71 \pm 0.02	1.147 \pm 0.047

Table 3. Results for the UBC dataset. We report the **FPR@95** metric similarly to previous works in local patch descriptors [7, 24]. SOSNet is the original result reported in [44], without data augmentation. We re-implemented SOSNet with data augmentation, denoted as SOSNet+ (*reimpl.*). The self-attention insertion are denoted by SOSNet+, SOA followed by the layer numbers after which SOA blocks are inserted. We follow [25]’s approach by performing each experiment \times three times and reporting the mean and standard deviation. Note that results from SOA_{4,5,6} are not reported as the network did not converge except when trained on the *liberty* subset. We observe that by utilising the second-order feature map re-weighting we outperform the state-of-the-art baseline SOSNet without extra supervision.

and descriptor distances generalises to local patch descriptors, and is not limited to image retrieval.

Datasets. Like most local patch descriptor works, we evaluate SOSNet with SOA blocks inserted on the UBC PhotoTour [9] and HPatches [6] datasets. UBC Phototour dataset is one of the most widely used dataset for evaluating local patch descriptor learning. It consists of three subsets, *liberty*, *notredame*, and *yosemite*. Models are trained on one subset and tested on the other two for evaluation. Similarly to previous works [7, 24], we follow standard protocol of [9] by reporting the false positive rate at 95% recall (**FPR@95**) on the 100K pairs provided.

HPatches dataset contains over 1.5 million patches extracted from numerous viewpoint and illumination changing scenes. We evaluate on the three tasks: *Patch Verification*, *Image Matching* and *Patch Retrieval*.

Impact of SOA at different layers. SOSNet [44] uses the L2-Net [43] architecture as the backbone. The architecture of L2-Net is shown in Table 4 where the network takes in a 32×32 grayscale patch and outputs a local descriptor with dimensionality of 128. The SOA block is insert-able at each intermediate feature map except for Layer-7, as the spatial dimension is reduced to 1×1 only. The earlier the SOA block(s) is inserted, the more fine-grained the spatial information is exploited. However this also comes at two costs. First, the computational complexity of the self-correlation multiplication from Equation 3 grows with $O(n^2)$ complexity, where n is the size of the spatial dimensions. Secondly the channel depth is shallower at earlier layers (32 at the first two layers vs. 128 at the final three layers) meaning that each spatial feature vector is less informative.

Layer	Kernel	Stride	Output shape $[h, w, c]$	Cumulative # Params.
1	3×3	1	32, 32, 32	288
2	3×3	1	32, 32, 32	9,216
3	3×3	2	16, 16, 64	18,432
4	3×3	1	16, 16, 64	36,864
5	3×3	2	8, 8, 128	73,728
6	3×3	1	8, 8, 128	147,756
7	8×8	1	1, 1, 128	285,984

Table 4. L2-Net [43] architecture. Note that we only show the convolutional kernel’s parameters and intermediate feature map dimension to assist discussion of non-local block insertions. Refer to Tian *et al.* [43] for the complete architecture including normalisation and activation layers.

To fully understand how second-order spatial information changes on patch description, we insert the SOA block described in Equations 3-4 into different feature layers of L2-Net [43] in Table 4.

The results reported in **FPR@95** on the UBC-PhotoTour [9] is shown in Table 5. We present results on each of the six test runs with various configuration of SOA insertions. We did not perform experiments involving SOA₁ and SOA₂ as similar to ResNet101, the 32×32 feature maps at Layers-1 & 2 add too much computational overhead, resulting in very slow training and we were unable to fit the mini-batch into available memory. We performed experiments on SOA insertion of one to three blocks from between Layers-3 to 7, giving the set of results {SOA₃, SOA₄, SOA₅, SOA₆, SOA_{3,4}, SOA_{3,5}, SOA_{4,5}, SOA_{4,6}, SOA_{3,4,5}, SOA_{4,5,6}}. To resolve potential noise, we follow the practice by Mukundan *et al.* [25] in performing three separate runs for each experiment and reporting the mean value and standard deviation.

HPatches Results

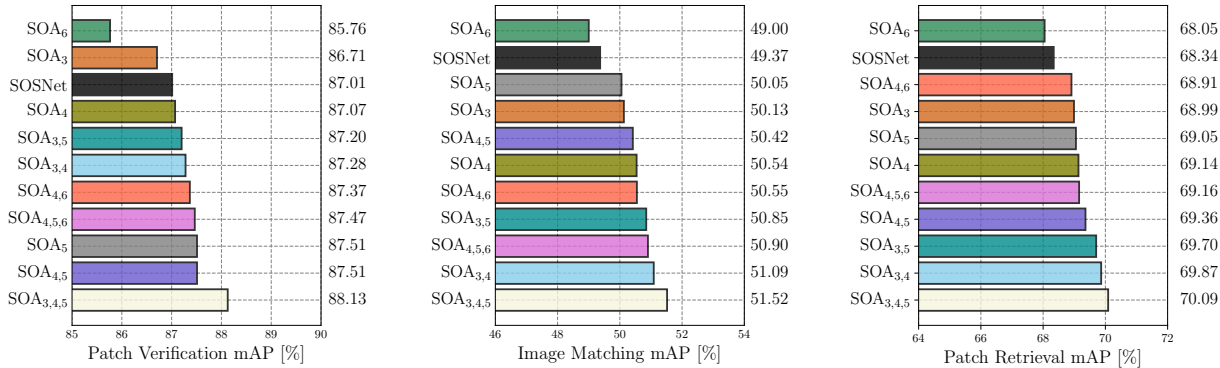


Figure 3. Performance evaluation on HPatches. 10 configurations of self-attention addition are compared with the SOSNet [44] backbone. Each configuration is denoted as SOA followed by the numbers indicating layers defined in Table 4 after which non-local blocks were inserted. Following common protocol we trained all models with the *liberty* subset of UBC and selected the model with the lowest average FPR@95. We used the parameter settings described in SOSNet [44] with a maximum number of 100 epochs. All training and testing were performed on patches resized to 32×32 .

Comparing the results of SOSNet with various SOAs inserted in Table 5, we can see that in general the SOA blocks increase the results slightly with few extra parameters. Interestingly, configurations with SOA₆ inserted perform noticeably worse when compared to the baseline. We suspect this is due to at this feature map level the spatial resolution is only down to 8×8 resulting in less second-order spatial correlation information exploitable, hence this poses a more difficult optimisation task for the SOA blocks at these higher-level feature maps. By comparing SOA_{3,4} with SOA_{3,5} and SOA_{4,5} with SOA_{4,6} we observe that SOA inserted at consecutive feature levels performs noticeably better. One potential explanation would be the immediate sharing of information across consecutive feature maps, allowing for better gradients into the SOA blocks to optimise for feature re-weighting. This also agrees with the improved performance of SOA_{4,5} over single SOA block insertion for ResNet101 in Section 5.1.

The results on HPatches are presented in Figure 3. We perform a similar practice in terms of SOA insertions but only on models trained with the *liberty* subset of the UBC dataset [9] following usual protocols. We select the best model according to the average **FPR@95** on *notredame* and *yosemite* for each SOA configuration and test on the HPatches dataset for *Verification*, *Matching* and *Retrieval* tasks. The results on all three tasks generally agree with that presented in Table 5. The addition of SOA₆ also led to a decrease of 0.64% in mAP across the three tasks. However an interesting observation is that best results in FPR@95 for UBC do not imply best results in HPatches. For example in Table 5 the mean FPR@95 of SOA_{3,4,5} is higher than that of baseline, but it out-performs all other SOA configurations across all three tasks in HPatches, scoring 2.06%, 2.15% and 1.75% improvement over the baseline SOSNet for *Verification*, *Matching* and *Retrieval* respectively. A po-

tential explanation to this contradiction could be the great contrast of patch type between the two datasets - UBC patches are in general very similar while HPatches contain patches of changing conditions. Overall, the improvement across different SOA insertions is consistent between UBC and HPatches, especially for *Patch Verification* in HPatches which is similar to the evaluation task in the UBC dataset.

The significant improvement brought by using three consecutive SAs could be attributed to the extra parameters, the sharing of spatial information between consecutive blocks, as well as the second-order spatial information across multi-scales (as Layers-3 & 4 have resolution of 16×16 while Layer-5 is 8×8).

Summary. We show that by combining second-order spatial information together with a second-order descriptor loss, the performance of descriptors is significantly improved for both local patches and full image retrieval tasks, as validated by results on several evaluation datasets. Hence it is evident that this exploitation of both kinds of second-order information is generalised to visual descriptors learning and can be easily implemented in an end-to-end fashion.

5.3. Qualitative retrieval results

We visualise (qualitatively) the effects of second-order feature map re-weighting in Figure 4. We observe that for features with spatial location at landmark-exclusive areas (columns (d) and (e)), the self-attention map at that location would look sparsely for the ‘silhouette’ of landmark locations within the full image it has learnt through training. On the other hand, when the feature is located within a landmark the self-attention would redirect the focus to highly informative features and other discriminant features that is not in its receptive field. This suggests that the second-order spatial re-weighting of feature maps through



Figure 4. Qualitative examples of second-order attention maps on the $\mathcal{ROxf}\text{-}\mathcal{RPar}$ dataset [34]. Each row depicts (a): the source image and four corresponding second-order attention maps at specific spatial locations (marked by pink stars). For each case, four spatial locations are selected – (b): pixel within the dominant landmark, (c): within a secondary landmark, (d): within the sky and (e): within another landmark-exclusive part other than the sky.

self-attention serves the purpose of “*suppressing weak features and strengthening strong features*”, leading to the increase in performance of descriptor generation. More examples are shown in A.1. Similar qualitative discussions for patches are presented in A.2.

We also compare direct results on image retrieval. For the example displayed in Figure 5, our proposed second-order method is able to re-weight the feature map to give higher activations on the strongest features and correctly retrieve the Top2-ranked candidates (as compared to only being correct at the 3rd and 4th ranks in GeM), contributing to a significant increase of 13.4% in average precision.

6. Implementation Details

GeM+SOLAR. We use the ResNet101-GeM [36] network pretrained on GL18² and fine-tuned our SOAs blocks on the loss from Equation 9. We trained for a maximum of 50 epochs on the same GL18 [42] dataset using Adam [20] with an initial learning rate of $1e^{-6}$ and exponential decay rate of 0.01. For each epoch 2000 anchors are randomly selected. Following [36], the triplet contains one positive

²cmp.felk.cvut.cz/cnnimageretrieval/data/networks/gl18/

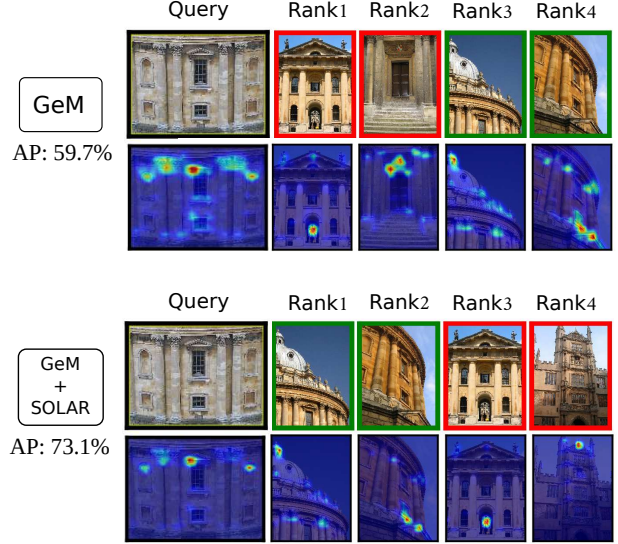


Figure 5. Example of performance between the baseline GeM descriptor (top) and our proposed second-order method (bottom) on a tough example in $\mathcal{ROxf}\text{-}\mathcal{Hard}$. The upper row for each method shows the query and the Top-4 ranked retrieval database images, with green and red borders denoting wrong and correct retrievals; the lower row shows the corresponding last feature map activation.

and 5 hard-negatives mined from 20,000 negative samples, each from a separate landmark. Training was performed with a batch-size of 8. We use $m = 1.25$ for the triplet loss and $\lambda = 10$ for the weighting of SOS loss.

SOSNet+SOAs. We re-implemented SOSNet [44] (and subsequent SOA insertions) with the details listed in the original paper to serve as a baseline for the ablation study.

All experiments are implemented in PyTorch [29]. For GeM+SOLAR[†], fine-tuning takes roughly 12 hours across 4 1080Ti GPUs. For SOSNET+SOAs, each training takes roughly 5 hours on a single 1080Ti GPU.

7. Conclusion

In this work, we propose SOLAR, a global descriptor that utilises second-order information through both spatial attention and descriptor similarity for large-scale image retrieval. We conduct a detailed study, both quantitative and qualitative on the impact of incorporating Second-Order Attention that learns to effectively re-weight feature maps and combine with the second-order information from descriptors similarity to produce better descriptors. We extend the SOLAR approach to local patch descriptors and showed that it improves upon current state-of-the-art descriptors without extra supervision, proving such second-order combination generalises to both descriptors. SOLAR achieves state-of-the-art performance on image retrieval benchmarks compared to similar *global single-pass* methods by a large margin and still outperforms *local aggregation* methods despite running at a fraction of both time and memory costs.

References

- [1] Relja Arandjelović, Petr Gronat, Akihiko Torii, Tomas Padilla, and Josef Sivic. NetVLAD: CNN architecture for weakly supervised place recognition. In *CVPR*, 2016. 2
- [2] Relja Arandjelović and Andrew Zisserman. Three things everyone should know to improve object retrieval. In *CVPR*, 2012. 2
- [3] Relja Arandjelović and Andrew Zisserman. DisLocation: Scalable descriptor distinctiveness for location recognition. In *ACCV*, 2014. 2
- [4] Artem Babenko and Victor Lempitsky. Aggregating deep convolutional features for image retrieval. In *ICCV*, 2015. 2, 4
- [5] Artem Babenko, Anton Slesarev, Alexandr Chigorin, and Victor Lempitsky. Neural codes for image retrieval. In *ECCV*, 2014. 2
- [6] Vassileios Balntas, Karel Lenc, Andrea Vedaldi, and Krystian Mikolajczyk. Hpatches: A benchmark and evaluation of handcrafted and learned local descriptors. In *CVPR*, 2017. 6, 12
- [7] Vassileios Balntas, Edgar Riba, Daniel Ponsa, and Krystian Mikolajczyk. Learning local feature descriptors with triplets and shallow convolutional neural networks. In *BMVC*, 2016. 3, 6
- [8] Herbert Bay, Tinne Tuytelaars, and Lue Van Gool. SURF: Speeded up robust features. In *ECCV*, 2006. 2
- [9] Matthew Brown, Gang Hua, and Simon Winder. Discriminative learning of local image descriptors. 33(1):43–57, 2011. 6, 7
- [10] David M. Chen, Georges Baatz, Kevin Köser, Sam S. Tsai, Ramakrishna Vedantham, Timo Pyhäläinen, Kimmo Roimela, Xin Chen, Jeff Bach, Marc Pollefeys, Bern Girod, and Radek Grzeszczuk. City-scale landmark identification on mobile devices. In *CVPR*, 2011. 2
- [11] Jia Deng, Wei Dong, Richard Socher, Li-Jia Li, Kai Li, and Li Fei-Fei. Imagenet: A large-scale hierarchical image database. In *CVPR*, 2009. 2
- [12] Yunchao Gong, Liwei Wang, Ruiqi Guo, and Svetlana Lazebnik. Multi-scale orderless pooling of deep convolutional activation features. In *ECCV*, 2014. 2
- [13] Albert Gordo, Jon Almazán, Jerome Revaud, and Larlus Diane. Deep image retrieval: Learning global representations for image search. In *ECCV*, 2016. 2, 4
- [14] Kaiming He, Xiangyu Zhang, Shaoqing Ren, and Jian Sun. Deep residual learning for image recognition. In *CVPR*, 2016. 2, 5
- [15] Hervé Jégou and Ondřej Chum. Negative evidences and co-occurrences in image retrieval: the benefit of pca and whitening. In *ECCV*, 2012. 2
- [16] Hervé Jégou, Matthijs Douze, and Cordelia Schmid. Hamming embedding and weak geometry consistency for large scale image search. In *ECCV*, 2008. 2
- [17] Hervé Jégou, Matthijs Douze, Cordelia Schmid, and Patrick Pérez. Aggregating local descriptors into a compact image representation. In *CVPR*, 2010. 2
- [18] Hervé Jégou, Florent Perronnin, Matthijs Douze, Jorge Sánchez, Patrick Pérez, and Cordelia Schmid. Aggregating local images descriptors into compact codes. In *TPAMI*, 2012. 2
- [19] Yannis Kalantidis, Clayton Mellina, and Simon Osindero. Crossdimensional weighting for aggregated deep convolutional features. In *ECCV*, 2016. 2, 4
- [20] Diederik P. Kingma and Jimmy Ba. Adam: A method for stochastic optimization, 2015. 8
- [21] Alex Krizhevsky, Ilya Sutskever, and Geoffrey E. Hinton. Imagenet classification with deep convolutional neural networks. In *NeurIPS*, 2012. 2
- [22] David G. Lowe. Distinctive image features from scale-invariant keypoints. In *IJCV*, 2004. 2
- [23] Krystian Mikolajczyk and Jiri Matas. Improving descriptors for fast tree matching by optimal linear projection. In *ICCV*, 2007. 4
- [24] Anastasiya Mishchuk, Dmytro Mishkin, Filip Radenović, and Jiri Matas. Working hard to know your neighbor's margins: Local descriptor learning loss. In *NeurIPS*, 2017. 3, 6
- [25] Arun Mukundan, Giorgos Tolias, and Ondřej Chum. Explicit spatial encoding for deep local descriptors, 2019. 6
- [26] Joe Yue-Hei Ng, Fan Yang, and Larry S. Davis. Exploiting local features from deep networks for image retrieval. In *CVPR Workshops*, 2015. 2
- [27] David Nistér and Henrik Stewénius. Scalable recognition with a vocabulary tree. In *CVPR*, 2006. 2
- [28] Hyeonwoo Noh, André Araujo, Jack Sim, Tobias Weyand, and Bohyung Han. Image retrieval with deep local features and attention-based keypoints. In *ICCV*, 2017. 2, 4
- [29] Adam Paszke, Sam Gross, Francisco Massa, Adam Lerer, James Bradbury, Gregory Chanan, Trevor Killeen, Zeming Lin, Natalia Gimelshein, Luca Antiga, Alban Desmaison, Andreas Kopf, Edward Yang, Zachary DeVito, Martin Raison, Alykhan Tejani, Sasank Chilamkurthy, Benoit Steiner, Lu Fang, Junjie Bai, and Soumith Chintala. PyTorch: An imperative style, high-performance deep learning library. In *NeurIPS*. 2019. 8
- [30] Florent Perronnin, Yan Liu, , Jorge Sánchez, and Hervé Poirier. Large-scale image retrieval with compressed fisher vectors. In *CVPR*, 2010. 2
- [31] Florent Perronnin, Jorge Sánchez, and Thomas Mensink. Improving the fisher kernel for large-scale image classification. In *ECCV*, 2010. 2
- [32] James Philbin, Ondřej Chum, Michael Isard, Josef Sivic, and Andrew Zisserman. Object retrieval with large vocabularies and fast spatial matching. In *CVPR*, 2007. 2, 4
- [33] James Philbin, Ondřej Chum, Michael Isard, Josef Sivic, and Andrew Zisserman. Lost in quantization: Improving particular object retrieval in large scale image databases. In *CVPR*, 2008. 2, 4
- [34] Filip Radenović, Ahmet Iscen, Giorgos Tolias, Yannis Avrithis, and Ondřej Chum. Revisiting oxford and paris: Large-scale image retrieval benchmarking. In *CVPR*, 2018. 2, 4, 5, 8, 11, 13

- [35] Filip Radenović, Giorgos Tolias, and Ondřej Chum. CNN image retrieval learns from BoW: Unsupervised fine-tuning with hard examples. In *ECCV*, 2016. 2
- [36] Filip Radenović, Giorgos Tolias, and Ondřej Chum. Fine-tuning CNN image retrieval with no human annotation. *TPAMI*, 2018. 2, 3, 4, 5, 8, 13
- [37] Shaoqing Ren, Kaiming He, Ross Girshick, and Jian Sun. Faster R-CNN: Towards real-time object detection with region proposal networks. In *NeurIPS*, 2015. 2
- [38] Jerome Revaud, Jon Almazán, Rafael Sampaio de Rezende, and César Roberto de Souza. Learning with average precision: Training image retrieval with a listwise loss. In *ICCV*, 2019. 2, 4
- [39] Karen Simonyan and Andrew Zisserman. Very deep convolutional networks for large-scale image recognition. In *arXiv:1409.1556*, 2014. 2
- [40] Josef Sivic and Andrew Zisserman. Video Google: A text retrieval approach to object matching in videos. In *ICCV*, 2003. 2
- [41] Vladyslav Sydorov, Mayu Sakurada, and Christopher H. Lampert. Deep fisher kernels end to end learning of the fisher kernel GMM parameters. In *CVPR*, 2014. 2
- [42] Marvin Teichmann, André Araujo, Menglong Zhu, and Jack Sim. Detect-to-Retrieve: Efficient regional aggregation for image search. In *CVPR*, 2019. 2, 3, 4, 5, 8
- [43] Yurun Tian, Bin Fan, and Fuchao Wu. L2-Net: Deep learning of discriminative patch descriptor in euclidean space. In *CVPR*, 2017. 2, 3, 6
- [44] Yurun Tian, Xin Yu, Bin Fan, Wu. Fuchao, Huub Heijnen, and Vassileios Balntas. SOSNet: Second order similarity regularization for local descriptor learning. In *CVPR*, 2019. 2, 3, 5, 6, 7, 8, 12
- [45] Giorgos Tolias, Yannis Avrithis, and Hervé Jégou. To aggregate or not to aggregate: Selective match kernels for image search. In *ICCV*, 2013. 2
- [46] Giorgos Tolias, Yannis Avrithis, and Hervé Jégou. Image search with selective match kernels: Aggregation across single and multiple images. In *IJCV*, 2015. 4
- [47] Giorgos Tolias, Teddy Furon, and Hervé Jégou. Orientation covariant aggregation of local descriptors with embeddings. In *ECCV*, 2014. 2
- [48] Giorgos Tolias, Ronan Sifre, and Hervé Jégou. Particular object retrieval with integral max-pooling of CNN activations. In *ICLR*, 2016. 2
- [49] Ashish Vaswani, Noam Shazeer, Niki Parmar, Jakob Uszkoreit, Llion Jones, Aidan N. Gomez, Lukasz Kaiser, and Illia Polosukhin. Attention is all you need, 2017. 1, 2
- [50] Xiaolong Wang, Ross Girshick, Abhinav Gupta, and Kaiming He. Non-local neural networks, 2018. 1, 2, 3
- [51] Bryan (Ning) Xia, Yuan Gong, Yizhe Zhang, and Christian Poellabauer. Second-order non-local attention networks for person re-identification, 2019. 1, 2
- [52] Tsun-Ti Yang, Duy-Kien Nguyen, Huub Heijnen, and Vassileios Balntas. DAME WEB: DynAmic MEan with Whitening Ensemble Binarization for landmark retrieval without human annotation. In *ICCV Workshops*, 2019. 4
- [53] Kwang Moo Yi, Eduard Trulls, Vincent Lepetit, and Pascal Fua. Lift: Learned invariant feature transform. In *ECCV*, 2016. 2
- [54] Han Zhang, Ian Goodfellow, Dimitris Metaxas, and Augustus Odena. Self-attention generative adversarial networks, 2019. 1, 2
- [55] Zhen Zhu, Song Xu, Mengde and Bai, Tengpeng Huang, and Xiang Bain. Asymmetric non-local neural networks for semantic segmentation, 2019. 1, 2

A. Appendix

A.1. Additional second-order attention maps on large images

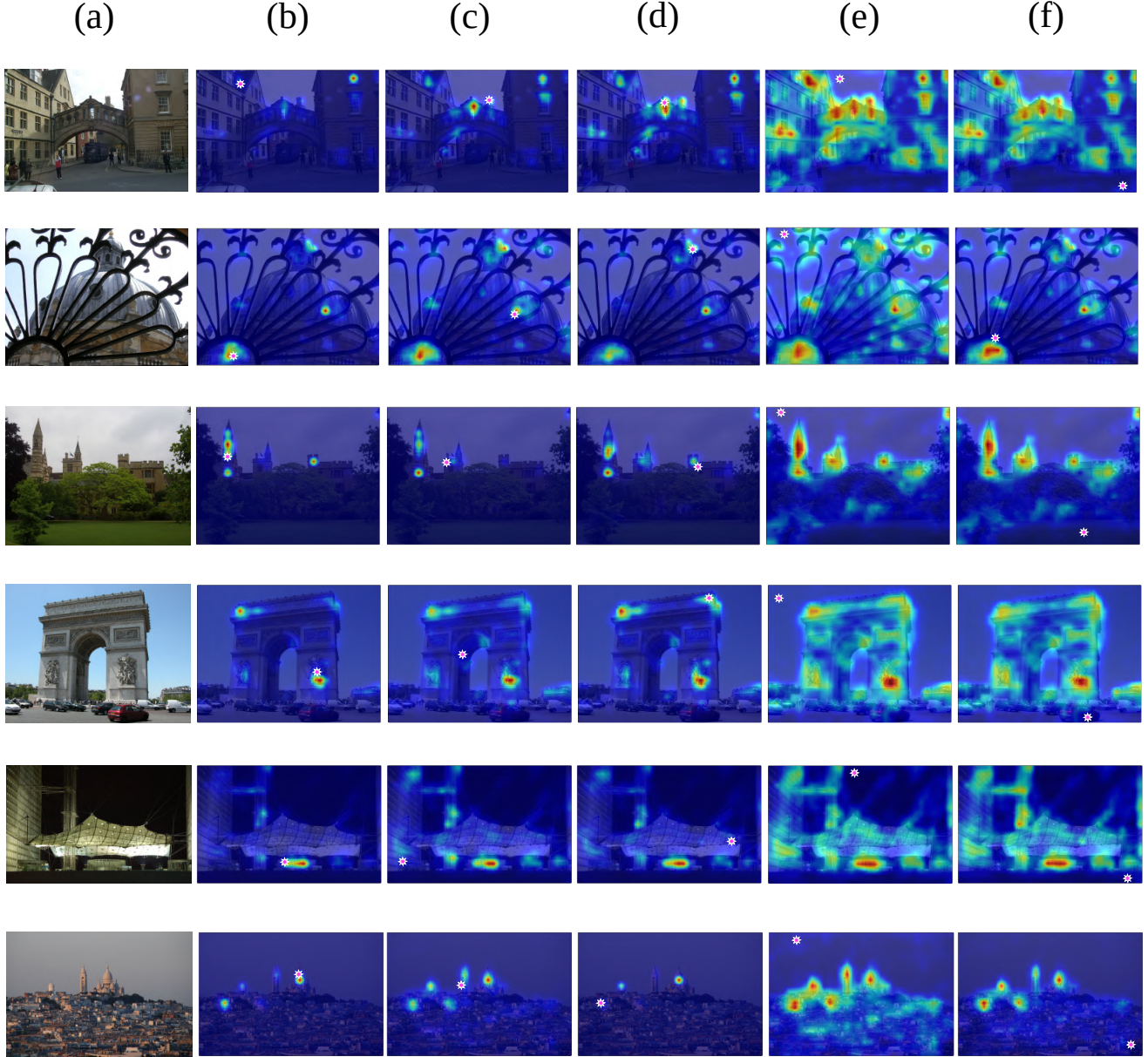


Figure 6. More qualitative examples of second-order attention maps on the $\mathcal{ROxf}\text{-}\mathcal{RPar}$ dataset [34], similar to that in Figure 4 in the paper. Each row depicts (a): the source image and four corresponding second-order attention maps at specific spatial locations (marked by pink stars). For each case, four spatial locations are selected – (b) - (d): pixels within different parts of prominent landmark(s) observed in the image, (e): within the sky and (f): within another landmark-exclusive part other than the sky.

A.2. Second-order attention maps on patches

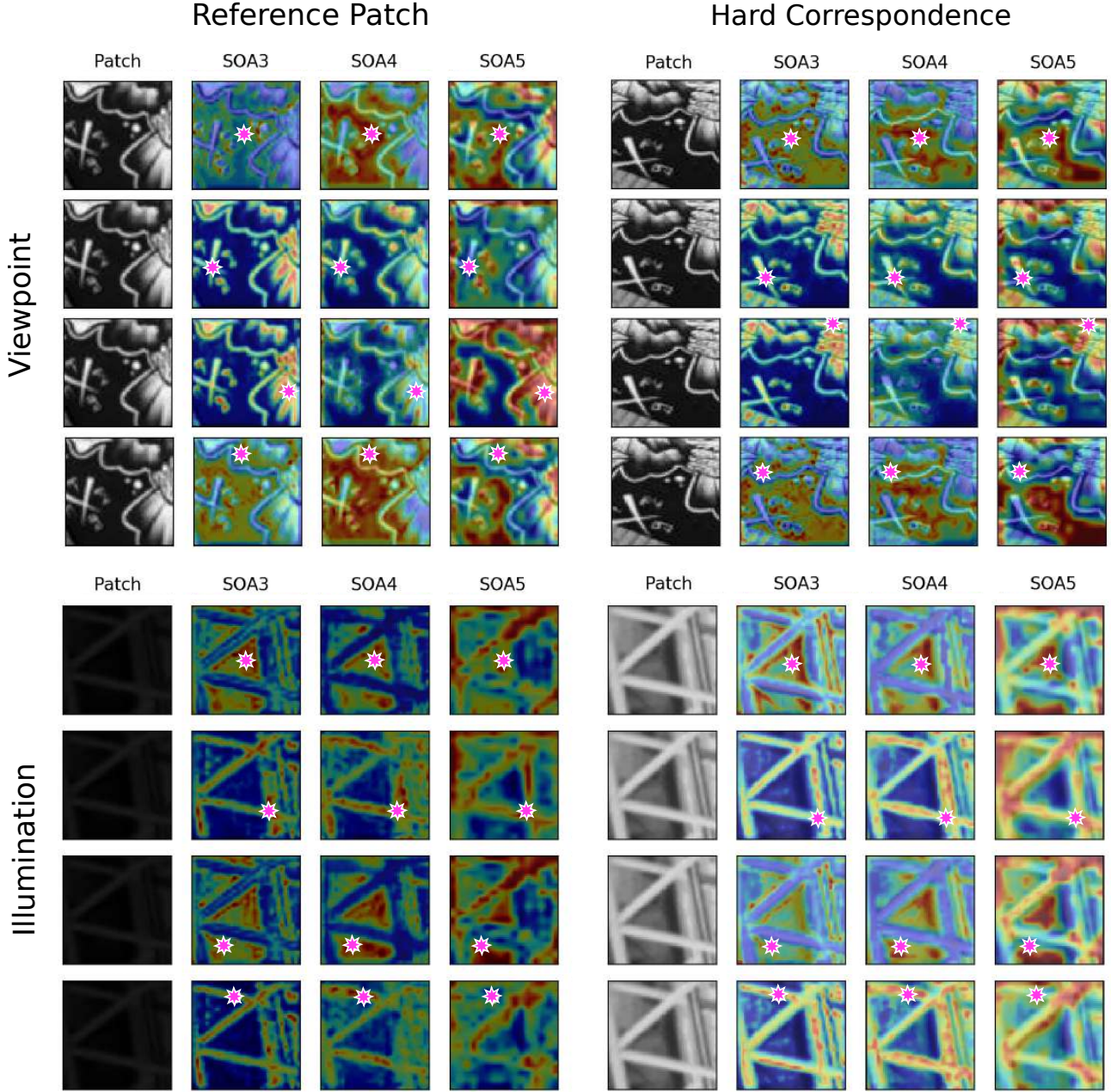


Figure 7. Second-order attention maps for HPatches [6]. **Left:** reference patch. **Right:** hard correspondence. **Top:** viewpoint changes to reference patch. **Bottom:** illumination changed to reference patch. For each case, we select four pixel locations (pink star) to display the attention maps of SOSNet[44]+SOA_{3,4,5} (which has the best results in HPatches evaluation).

Figure 8 above visualises the second-order attention maps (similar to Figure 4 in the paper) on two example patches from HPatches [6]. We show two examples reference patches and each a ‘hard’ corresponding patch from a sequence with viewpoint (top) and illumination changes (bottom). Firstly we observe that in contrast to large images, the self-attention at a given spatial location focuses on

similar / connected structures within the patch. This is due to much less semantic (and colour) information in patches compared to large images. Secondly we also observe that the attention maps are invariant to both viewpoint and illumination changes. As we compare the reference patch to the hard correspondence, the attentions between are consistent across all three levels in SOA_{3,4,5}.

A.3. Qualitative retrieval comparison between GeM and SOLAR



Figure 8. Four examples of performance between the baseline GeM descriptor (top) and our proposed SOLAR descriptor in the hard protocol of $\mathcal{ROxf}\text{-}\mathcal{RPar}$ [34]. The upper and lower rows for each example show the query and the Top-9 ranked retrieval database images for GeM [36] and SOLAR respectively, with green and red borders denoting correct and wrong retrievals. Notice, especially for the Top-5 ranks the higher number of correct (green) retrievals by SOLAR vs. GeM.